Hydrophobic interactions leading to a complex interplay between bioelectrocatalytic properties and multilayer meso-organization in layer-by-layer assemblies

M. Lorena Cortez,[ab] Nicolás De Matteis,[b] Marcelo Ceolín,[a] Wolfgang Knoll,[c] Fernando Battaglini*[b] and Omar Azzaroni*[a]

The present study explores the development of mesostructured bioelectrochemical interfaces with accurate compositional and topological control of the supramolecular architecture through the layer-by-layer assembly of ternary systems based on poly(allylamine) containing an osmium polypyridyl complex (OsPA), an anionic surfactant, sodium dodecyl sulfate (SDS) or sodium octodecyl sulfate (ODS), and glucose oxidase (GOx). We show that the introduction of the anionic surfactant allows a sensitive increase of the polyelectrolyte and the enzyme uptake at pH 7.0, enhancing its catalytic behavior in the presence of glucose as compared to the surfactant-free system $(OsPA/GOx)_n$ constructed at the same pH. Structural characterization of the multilayer films was performed by means of grazing-incidence small-angle X-ray scattering (GISAXS), which showed the formation of mesostructured domains within the composite assemblies. Experimental results indicate that the balance between ionic and hydrophobic interactions plays a leading role not only in the construction of the self-assembled system but also in the functional properties of the bioactive interface. The structure of the ternary multilayered films depends largely on the length of the alkyl chain of the surfactant. We show that surfactants incorporated into the film also play a role as chemical entities capable of tuning the hydrophobicity of the whole assembly. In this way, the deliberate introduction of short-range hydrophobic forces was exploited as an additional variable to manipulate the adsorption and coverage of protein during each assembly step. However, the integration of long-chain surfactants may lead to the formation of very well-organized interfacial architectures with poor electron transfer properties. This, in turn, leads to a complex trade-off between enzyme coverage and redox wiring that is governed by the meso-organization and the hydrophobic characteristics of the multilayer assembly.

Introduction

Construction of self-assembled systems into thin film formats and immobilization of functional molecules on suitable surfaces are often required for implementation of practical devices that address specific applications.[1,2] A prerequisite for the construction of such functional interfaces is the development of methods for integrating molecular components into well-ordered assemblies[3,4]

with a well-defined supramolecular architecture.[5] Therefore, such interfacial architectures require strict control over the organization at the nanometer scale, and therefore it is essential to study and develop methods for the controlled assembly of multicomponent nanostructures on surfaces.[6] Research efforts on this matter are often referred to as "*nanoarchitectonics*", a term popularized by Ariga and co-workers.[7–10]

During the last decade there have been numerous examples of functional supramolecular nanosystems comprising organized monomolecular films on surfaces.[11,12] However, a significant body of literature demonstrated that multilayer films can enhance the properties of monomolecular films[13] and offer the chance to create interfaces possessing functional groups at controlled sites in three-dimensional arrangements.[14–16] Within this framework, layer-by-layer (LbL) assembly has emerged as a very versatile method for fabricating structured and functional thin films on solid substrates. First proposed by Iler in 1966, and then

[a] *Instituto de Investigaciones Fisicoquímicas Teóricas y Aplicadas (INIFTA), Universidad Nacional de La Plata, CONICET, CC 16 Suc. 4, (1900) La Plata, Argentina. E-mail: azzaroni@inifta.unlp.edu.ar; Web: http://softmatter.quimica.unlp.edu.ar*

[b] *INQUIMAE - Departamento de Química Inorgánica, Analítica y Química Física, Facultad de Ciencias Exactas y Naturales, Universidad de Buenos Aires, Ciudad Universitaria - Pabellón 2, C1428EHA Buenos Aires, Argentina. E-mail: battagli@qi.fcen.uba.ar*

[c] *Austrian Institute of Technology (AIT), Donau-City-Strasse 1, 1220 Vienna, Austria*

20844 | *Phys. Chem. Chem. Phys.*, 2014, **16**, 20844–20855

This journal is © the Owner Societies 2014

rediscovered by Decher and Hong in the early 1990s,[17] the LbL electrostatic adsorption is nowadays firmly established as a general method for alternately depositing dense monolayers of charged molecules onto oppositely charged surfaces.[18,19] The power of the approach relies on the attractive forces between oppositely charged molecules, namely polyelectrolytes, proteins, nanoparticles, *etc.* LbL assembly of multilayer films involves the construction of complex composite materials with nanoscale precision in film thickness and composition, enabling the development of novel structures and devices with properties tailored by controlling the molecular arrangement.[18,20–22] These advanced preparative strategies are essential in the case of bioelectrochemical interfaces provided that electrical contacting of redox proteins with electrodes is the cornerstone of enzymatic electrodes for biosensor applications and biofuel cells' design.[23–27] Different supramolecular strategies to electrically contact redox proteins and electrodes have been reported, including the LbL integration enzymes and redox polyelectrolytes.[28]

The seminal work by Kotov[29] demonstrated that strong electrostatic attraction of opposite charges located on the substrate and on the building block to be assembled does not guarantee the formation of multilayers. Along with pure electrostatic forces, hydrophobic interactions have to be considered when designing LbL assemblies. Short-range hydrophobic forces were identified as one of the important factors determining the ability of a compound to self-assemble *via* the LbL technique and consequently they should be considered as a major driving force in layer-by-layer deposition.

The preparation of LbL assemblies integrating surfactants and polyelectrolytes is very appealing since these building blocks would provide a broad set of interactions to the supramolecular assembly.[30] The association between oppositely charged polymers and surfactants in water is driven by both electrostatic and hydrophobic interactions and many factors can influence the properties of these assemblies, *e.g.* molecular weight, charge density, hydrophobicity, backbone rigidity, *etc.*[31]

Indeed, it has been demonstrated that in polyelectrolyte films, fine-tuning of surface wettability by using surfactants may provide additional physical or chemical robustness.[32] On the other hand, long-chain surfactant assemblies can function as hierarchical structure-directing agents at both the meso- and microstructural levels.[33–35] Exciting opportunities are revealed when we think in this manner. Surfactant–polyelectrolyte interactions provide a complementary perspective from which one can consider the manipulation of the supramolecular ordering, and ultimately control the functional features of interfacial architecture *via* dimensional intra- and interlayer control.[36,37]

LbL assemblies displaying mesostructural organization are not trivial compared to typical surfactant-free LbL polyelectrolyte assemblies. As extensively demonstrated by Jonas and co-workers, employing X-ray techniques, the internal structures of most polyelectrolyte-based electrostatic self-assemblies are highly disordered.[38,39] Sequentially deposited layers of polyelectrolytes interpenetrate so strongly that the compositional fluctuation perpendicular to the surface is completely smoothed out. This leads to a situation in which many LbL thin film assemblies should be considered as macromolecular blends of polyelectrolytes.[40] The lack of true layering and mesostructural organization in LbL films may be a limitation of the technique, because well-organized multilayers are required for a number of applications requiring the precise placement of active functional groups in confined layers.[41,42]

Despite the attractive features of surfactant–polyelectrolyte complexes there appears to be extremely few examples of surfactant-based LbL assemblies in the literature[43] and, to our knowledge, functionally mesostructured surfactant–polyelectrolyte LbL assemblies have not been previously anchored onto electrode supports. In addition, although some functional films have been fabricated by the LbL assembly of polyelectrolyte–surfactant complexes,[44] the structural tailoring of LbL-assembled films using surfactants as building blocks is far from being well investigated. Herein we describe the stepwise construction of a novel kind of self-assembled mesostructured multilayers on the basis of the integration of surfactants within the inner structure of the multilayer assembly. A quartz crystal microbalance (QCM) and cyclic voltammetry (CV) have been used for estimating the protein and redox polyelectrolyte coverage and for monitoring and quantifying the growth process and the evolution of the redox connectivity upon increasing the number of multilayers. The present work aims to understand the role of hydrophobic interactions in the deposition behavior and structural and functional tailoring of the surfactant-containing LbL assembled films. Our results reveal an interesting trade-off between protein and polyelectrolyte coverage (manipulated by surface hydrophobicity) and bioelectrocatalytic activity (dominated by meso-organization) that is affected by the presence of the surfactant. To the best of our knowledge this is the first report based on experimental results describing how hydrophobic interactions affect the functional and structural characteristics of LbL assemblies.

Materials and methods

Sodium 3-mercapto-1-propanesulfonate (MPS), sodium dodecyl sulfate, and octadecyl sulfate were purchased from Aldrich. Glucose oxidase was from Biozyme. All other reagents were of analytical grade. The synthesis of poly(allylamine) containing a pyridine based osmium complex (OsPA) is described elsewhere.[45] Self-assembled multilayers were obtained by immersing the gold surface subsequently in each of the corresponding solutions. Depending on the dipping step, the following conditions were used: *thiol adsorption*: clean gold electrodes were immersed in a 20 mM 3-mercapto-1-propanesulfonate solution in 10 mM H_2SO_4 for 60 min. *OsPA adsorption*: the modified electrodes were immersed in 50 mM Tris solution (pH 7.0) containing 0.4% w/v OsPA for 10 min. *Anionic alkyl surfactant adsorption*: the electrode was immersed in 1% w/v SDS or 0.5 mM ODS solution in water for 10 min. *GOx adsorption*: the electrode was immersed in 1 μM GOx solution in 50 mM HEPES buffer (pH 7.0) for 10 min. In the case of GISAXS experiments silicon surfaces were oxidized and modified with

This journal is © the Owner Societies 2014

Phys. Chem. Chem. Phys., 2014, **16**, 20844–20855 | 20845

polyethyleneimine (PEI) as a primer and thereafter the process was the same as that for gold electrodes.

Electrochemical experiments were carried out using a potentiostat (TEQ-02). The system consisted of a working electrode, a platinum mesh counter electrode, and an Ag/AgCl reference electrode. Quartz crystal microbalance experiments were carried out in a 5 MHz QCM-200 Stanford Research Systems setup. The variation in the resistive parameter of the Butterworth–Van Dyke electrical equivalent circuit that represents the composite quartz crystal resonator loaded with the film, ΔR, in all cases is negligible compared to the inductive quartz impedance component, ΔX_L. Therefore, the films behave as acoustically thin in the gravimetric regime and the mass uptake was calculated in each case using the Sauerbrey equation.[46,47] Advancing water contact angle experiments were carried out on a KSV CAM200 optical contact angle meter. GISAXS measurements were performed at the D10A-XRD2 beamline of Laboratório Nacional de Luz Síncrotron (LNLS, Campinas, Brazil). A monochromatic beam of 7689 eV (λ = 1.6124 Å) was used to perform the experiments. Large size (2×2 cm^2) silicon wafers were used as GISAXS sample substrates. GISAXS scattering intensities were recorded using a Pilatus 100 K detector (DECTRIS Ltd – Baden, Switzerland) at a distance of 631 mm from the sample (calibration: 64 pixel per degree). Exposure times under these conditions ranged from 60 s to 80 s depending on the contrast and sample quality. The beam size was 150 μm × 4 mm. Lamellar spacings were determined according to the procedure described by Di et al.[48]

Results and discussion

Multilayer films were fabricated by alternating deposition of redox-active Os-tagged poly(allylamine) hydrochloride, sodium dodecyl sulfate and glucose oxidase (GOx). The protocol leading to the layer-by-layer formation of multicomposite molecular assemblies comprised of Os-PA/SDS/GOx multilayers is schematically outlined in Fig. 1.

First, quartz crystal microbalance (QCM) experiments[49] were conducted to confirm the regular formation of (OsPA/SDS/OsPA/GOx)$_n$ multilayers on planar supports. Integration of each building block was recorded online in a liquid cell. The electrode surface was primed with a sodium 3-mercapto-1-propanesulfonate self-assembled monolayer which was chemisorbed from an aqueous solution. Alternating layers of OsPA, SDS and GOx were then deposited using solutions with concentrations, 0.4% w/v, 1% w/v and 1 μM, respectively. The washing steps following the adsorption of each building block were performed using Milli-Q water. The buildup of multilayers can be seen in Fig. 2, which shows the mass of the film as a function of layer number. The repetition of the adsorption of OsPA, SDS and GOx in a cyclic fashion led to a multilayer assembly. The film made from alternate layers of OsPA/SDS/OsPA/GOx shows an increase in the film mass as a function of layer number. Different sets of experiments of film formation showed that the growth of such films is not strictly linear, but fully achievable with good reproducibility. In particular, it is systematically observed that the assembly of SDS onto the OsPA layer leads
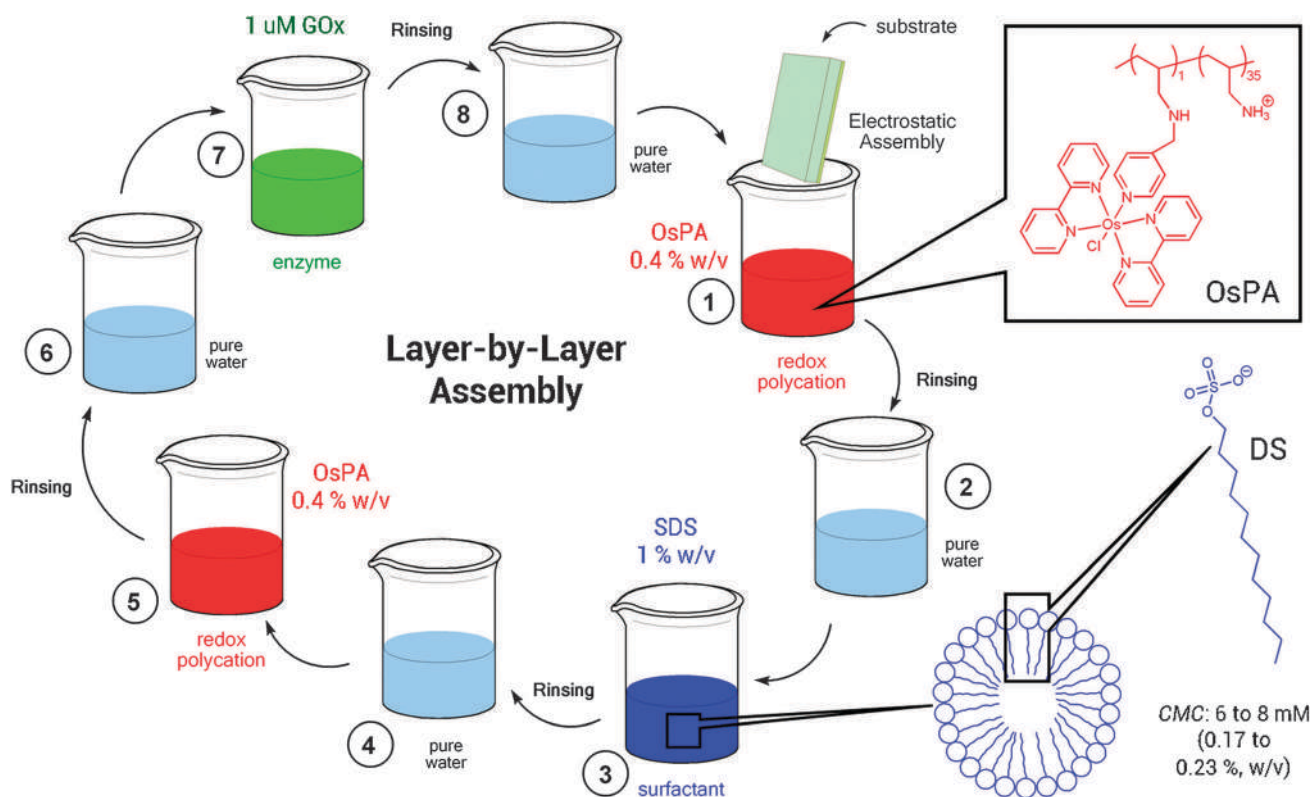

Fig. 1 Schematic of the film deposition process. Steps 1 to 5 represent the formation of OsPA/SDS/OsPA layers whereas step 7 represents the integration of glucose oxidase within the assembly. The figure also describes the chemical structure of the surfactant and the redox polyelectrolyte.
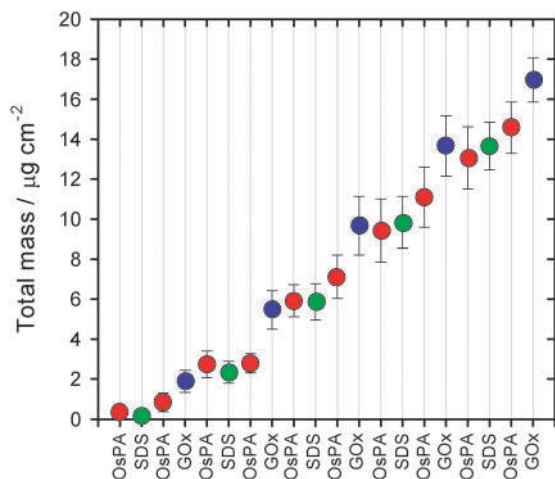
20846 | Phys. Chem. Chem. Phys., 2014, 16, 20844–20855

This journal is © the Owner Societies 2014

Fig. 2 Total deposited mass as a function of layer number for (OsPA/SDS/OsPA/GOx)$_n$ assemblies. Different colors were used to indicate the assembly of OsPA (red), SDS (green) and GOx (blue) in the multilayered film.

to a reduced mass increase as compared to the rest of the assembling layers. Recently, Rahim *et al.*[50] showed that SDS is able to remove polyelectrolyte chains that are loosely integrated in layer-by-layer films. Our results might indicate that the present system behaves in a rather similar way and the assembly of SDS could remove OsPA chains weakly adsorbed on the outermost layer of the film. In addition, we should consider that multilayer growth was tracked by *in situ* QCM.[51–53] Hence, the adsorption of SDS may also lead to partial dehydration of the film with the concomitant decrease of the mass viscoelastically coupled to the quartz crystal.

In order to better understand the changes produced by this new assembling strategy integrating SDS, *i.e.* (OsPA/SDS/OsPA/GOx)$_n$, all the experiments were always compared to (OsPA/GOx)$_n$ self-assembled systems contemporarily constructed. For a system of (OsPA/SDS/OsPA/GOx)$_n$ multilayers the amount of GOx incorporated into the multilayer films containing the SDS is *ca.* 3.5 times higher than in a comparable system of SDS-free multilayers. These meaningful differences in GOx incorporation can be observed in Fig. 3a. SDS-containing films add 2.8 µg cm^{-2} of GOx per dipping cycle whereas SDS-free films only incorporate 0.82 µg cm^{-2} during each self-assembly step. This clearly demonstrates that the relative amount of GOx incorporated into the systems of layered (OsPA/SDS/OsPA/GOx)$_n$ is higher than in the classically assembled films. Hence, the current approach provides an alternative means to enhance the integration of proteins in electrostatically LbL assembled multilayers.[54]

In both cases GOx is adsorbed atop the cationic OsPA layer *via* electrostatic interactions; however, it is evident that hydrophobic interactions within the film play a dominant role in the case of films containing SDS. For instance, changes in surface hydrophilicity are evident in SDS-containing multilayers. Contact angles of OsPA-capped films in (OsPA/SDS/OsPA/GOx)$_n$ and (OsPA/GOx)$_n$ multilayers are 104° and 57°, respectively. Concomitantly, wetting measurements and QCM data reveal that hydrophobic surfaces of opposite charge to that of the protein were found to be more effective at promoting protein adsorption.
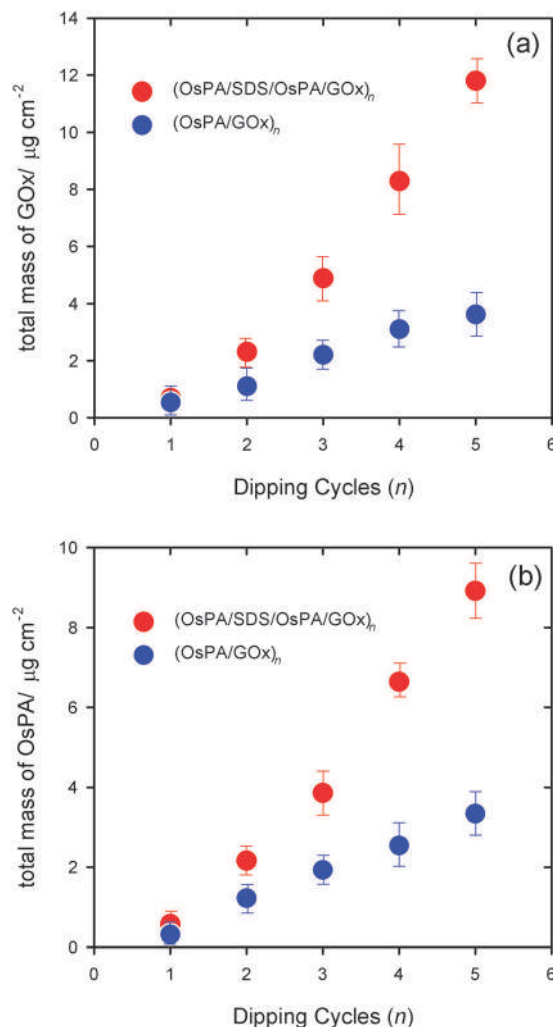

Fig. 3 (a) Total glucose oxidase (GOx) mass contained in (OsPA/SDS/OsPA/GOx)$_n$ (red)and (OsPA/GOx)$_n$ (blue) multilayers as a function of dipping cycle (*n*). (b) Total osmium polypyridyl complex-modified polyelectrolyte (OsPA) mass contained in (OsPA/SDS/OsPA/GOx)$_n$ (red)and (OsPA/GOx)$_n$ (blue) multilayers as a function of dipping cycle (*n*).

A rather similar scenario is observed when we analyze the QCM data corresponding to the integration of OsPA in the SDS-free and SDS-containing multilayer assemblies separately (Fig. 3b). The amount of OsPA incorporated into (OsPA/SDS/OsPA/GOx)$_n$ and (OsPA/GOx)$_n$ multilayers during each dipping cycle is 2.1 and 0.74 µg cm^{-2}, respectively. It is worthwhile mentioning here that in (OsPA/SDS/OsPA/GOx)$_n$ multilayers each dipping cycle involves two OsPA assembly steps (see Fig. 1). The ratio between the OsPA content in conventional and SDS-containing multilayers is 2.8. This experimental observation suggests that hydrophobic interactions also play an important role in determining the amount of redox polyelectrolyte that is adsorbed on the modified surface. The association between oppositely charged polymers and surfactants in water is driven by both electrostatic and hydrophobic interactions.[55] The best way to illustrate the critical role of hydrophobicity is to compare the wettability of substrates onto which OsPA is assembled. In our

This journal is © the Owner Societies 2014

Phys. Chem. Chem. Phys., 2014, **16**, 20844–20855 | 20847

case GOx-capped (OsPA/GOx)$_n$ films display contact angle (CA) values close to 40° whereas SDS-capped (OsPA/SDS/OsPA/GOx)$_n$ multilayers exhibit a very pronounced hydrophobic character, CA $\sim$ 115°. The increasing hydrophobicity of the surface further supports the finding that the changes in the adsorption characteristics are influenced by the presence of SDS on the surface of the film. The anionic headgroups of the SDS molecules bind to the positive sites of the OsPA layer, leaving the hydrophobic hydrocarbon tails exposed, which would increase the hydrophobicity of the OsPA–SDS outer layer. Notably, OsPA assembly on SDS-capped surfaces also leads to hydrophobic surfaces, CA $\sim$ 104°. The increase in the contact angle for the capping OsPA layer might indicate that the hydrophobic alkyl chains of SDS are present on the outermost polyelectrolyte layer. We hypothesize that when OsPA is added onto a SDS underlayer, the alkyl chains of the surfactant likely interpenetrate through the new polyelectrolyte layer, causing an increase in surface hydrophobicity. A similar observation was reported by Johal *et al.* for the adsorption of SDS on poly(ethylenimine) in multilayered thin films.[56] Within this context we should also emphasize that incubation of GOx in the presence of SDS yields cooperative (hydrophobic) binding with retention of activity.[57] Considering these aspects, it is plausible to consider that the effective SDS integration in the self-assembled system could be also ascribed to the interaction with hydrophobic pockets on the surrounding enzymes.

Then, we proceeded to examine and compare the electrochemical properties of both types of assemblies. Typical cyclic voltammograms for multilayers assembled during 1–4 dipping cycles are depicted in Fig. 4a. Evidently, an almost linear increase in the content of electroactive units as a function of dipping cycles is observed. Cyclic voltammograms exhibit characteristic features of redox surface processes with a peak separation of less than 15 mV and a full width at half maximum (FWHM) slightly larger ($\sim$110 mV) than the theoretical value for an ideal Nernstian surface layer, *i.e.*: 90.6 mV for a one electron transfer process. This fact might reflect repulsive interactions of the osmium complex in the multilayer matrix.[58] As described by several authors the redox potential depends on the local electrostatic environment due to Donnan potential contribution. In our case we observed no differences in redox potentials between films assembled in the presence or in the absence of SDS. Fig. 4b shows that the integrated charge also increases with the number of dipping cycles or self-assembled layers. Charge propagation through the consecutive layers takes place by electron hopping between adjacent osmium redox centres in the polymer in a diffusion-like process. The electrochemical charge involved in the voltammetric response of the supramolecular assemblies provides a quantitative estimation of the density of electroactive sites connected or "wired" to the electrode.[42] Data displayed in Fig. 4b reveal that both types of assemblies, (OsPA/SDS/OsPA/GOx)$_n$ and (OsPA/GOx)$_n$, present a similar amount of "wired" redox centers connected to the underlying gold electrode. On the other hand, as discussed above, QCM data indicate that the amount of OsPA in (OsPA/SDS/OsPA/GOx)$_n$ is 2.8 times higher than in (OsPA/GOx)$_n$ multilayers. By comparing the information derived from cyclic voltammetry and QCM we can infer that only 35% of Os centers are
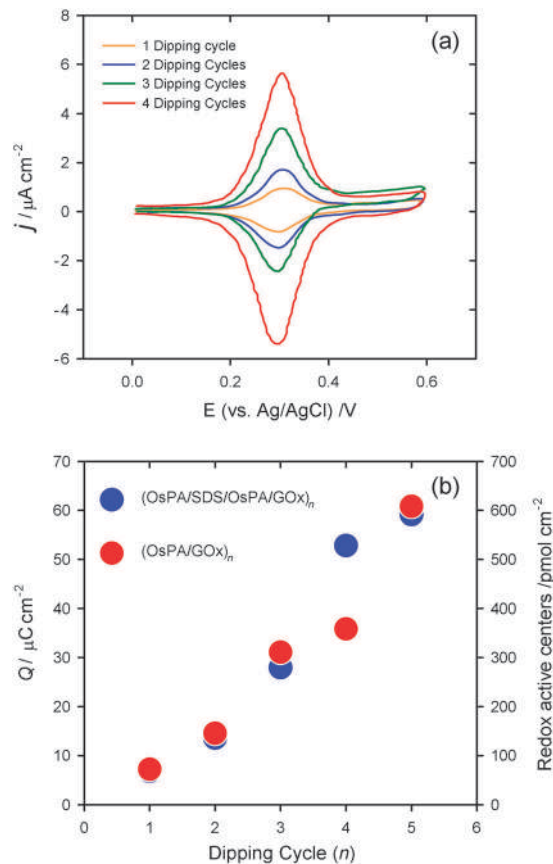

Fig. 4 (a) Cyclic voltammograms of self-assembled (OsPA/SDS/OsPA/GOx)$_n$ multilayers built up over several dipping cycles (*n*). Scan rate: 10 mV s^{-1}. Supporting electrolyte: 50 mM HEPES, 0.2 M KNO$_3$ buffer solution at pH 7.0. (b) Representation of the electrochemical charge associated with the oxidation–reduction of the osmium centers incorporated into the supramolecular assembly as a function of the number of dipping cycles (*n*). Error bars are comparable to the data symbol size.

connected to the electrode support in the (OsPA/SDS/OsPA/GOx)$_n$ multilayers. It is evident that the presence of SDS alters the redox connectivity of the supramolecular assembly. As we already mentioned the alkyl chains of SDS might interpenetrate through the OsPA layer precluding the hopping between Os centers.

In addition, the presence of surfactants in the supramolecular assembly might also introduce drastic changes in the inner structure of the multilayered film with their concomitant effects on the "wiring" efficiency. Therefore, a non-destructive method is required for the quantitative structural analysis of the multilayer thin films deposited on substrates in the out-of-plane and in-plane directions of the film. Recently, grazing-incidence X-ray scattering has emerged as a very powerful technique for characterizing both surface and internal structures in supported thin films.[59,60] In particular, GISAXS is well suited for structural characterization of thin films due to a highly intense scattering pattern with high statistical significance always obtained, even for films of nanoscale thickness, because the X-ray beam path-length through the film plane is sufficiently long.[61] Unlike local techniques, like atomic force microscopy, statistics derived from GISAXS investigations are representative of the most dominant

20848 | *Phys. Chem. Chem. Phys.*, 2014, **16**, 20844–20855

This journal is © the Owner Societies 2014

structural features of the sample as a whole. In our studies, experimental parameters were chosen such that the dominant contributions to X-ray scattering arise from the bulk of the LbL films.

GISAXS patterns obtained from (OsPA/GOx)$_3$ and (OsPA/SDS/OsPA/GOx)$_3$ films are shown in Fig. 5. Direct visual comparison of both GISAXS patterns eloquently reveals the absence of meso-organization in the case of (OsPA/GOx)$_3$ films as well as the presence of mesostructured domains in the multilayers containing SDS. GISAXS characterization of (OsPA/SDS/OsPA/GOx)$_3$ films show a bright region (highest intensity) in the direction q_z (for $q_y \rightarrow 0$) and the presence of an appreciable intensity halo (Fig. 5b). This suggests that while there are lamellar domains oriented parallel to the substrate there is a strong contribution of multioriented lamellar domains (randomly oriented small domains). This GISAXS pattern closely resembles those obtained in phase segregated Nafion films in which the halo is often referred to as the "ionomer ring".[62,63] It is evident that the integration of SDS in the assembly introduced mesostructural order in the supramolecular system; however, meso-organization in large domains is rather poor.

On the other hand, it is well known that water uptake may lead to swelling of hydrophilic polyelectrolyte domains in phase-segregated materials.[64,65] Considering that aqueous environments represent a more realistic scenario for studying the function–structure properties of these systems we assessed the influence of water on the lamella dimensions. To this end, we performed GISAXS experiments at various humidity levels until reaching saturation (Fig. 6). We observed a slight increase in lamellar spacing (l) from 4.08 to 4.22 nm upon increasing the relative humidity from 1 to 75%. Then, further increase of RH to 95% led to a slight decrease in l, 4.16 nm. In few words, the lamellar domains experience only slight dimensional changes ($\sim$2%) in the presence of water. These experiments indicate
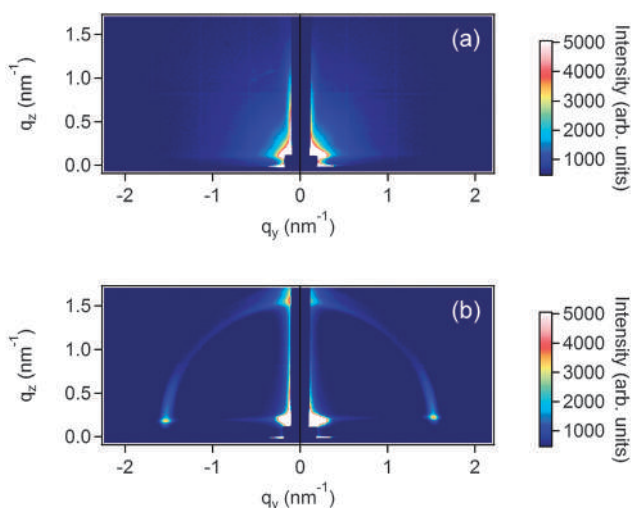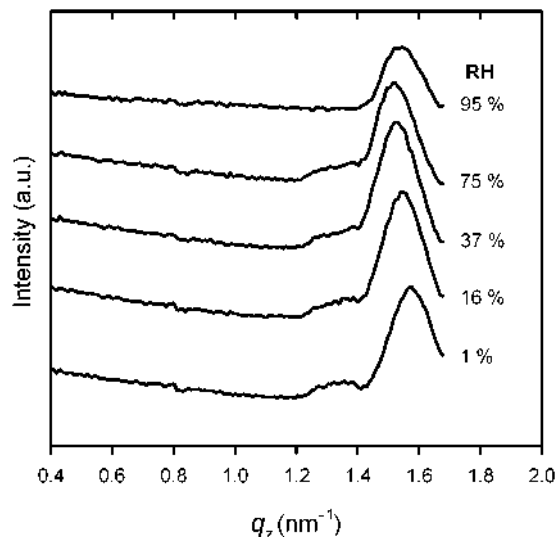

Fig. 6 Out-of-plane scattering profiles extracted along the q_z direction (at q_y = 0.2 nm^{-1} with Δq_z width corresponding to ± 0.01 nm^{-1}) from the GISAXS patterns of (OsPA/SDS/OsPA/GOx)$_3$ multilayers obtained under different humidity conditions.

that the way in which the redox centers accommodate during the self-assembly process is preserved after immersion in water.

So far, we have demonstrated that the integration of the surfactant in the LbL can be exploited as mesomorphic structure-directing agents as well as a driving force to increase the adsorption of the enzyme through hydrophobic interactions.[66,67] Next, we will study the bioelectrocatalytic features of (OsPA/SDS/OsPA/GOx)$_n$ assemblies in the presence of the enzyme substrate. Their voltammetric response eloquently illustrates the responsiveness of the GOx-containing supramolecular assembly to the presence of the glucose in the surroundings of the electrode surface. Fig. 7 shows the amperometric responses of (OsPA/SDS/OsPA/GOx)$_5$ and (OsPA/GOx)$_5$ enzyme electrodes in the presence of the substrate. Even though the (OsPA/GOx)$_5$ enzyme electrode yields a well-defined amperometric response, the supramolecular array composed of (OsPA/SDS/OsPA/GOx)$_5$ reveals a significant anodic current implying that glucose is efficiently oxidized by the enzyme-containing mesostructured redox-active assembly. Control experiments (not shown) confirmed that in the absence of Os tethers on the polyelectrolyte layers, no amperometric responses are observed in any of the enzyme electrode configurations, although the immobilized enzymes exhibit biocatalytic activity. To better describe the influence of the GOx overlayers on the electrocatalytic activity of the assembly we have plotted the increase of the current density developed through the electrochemical interface upon increasing the number of GOx monolayers assembled on the electrode surface (Fig. 8). As expected, the glucose responsiveness of the interfacial assemblies is proportional to the amount of immobilized enzyme. However, we observe a remarkable increase in the catalytic response of (OsPA/SDS/OsPA/GOx)$_n$ assemblies with respect to the traditional (OsPA/GOx)$_n$ LbL multilayers. As previously discussed the introduction of a negatively charged surfactant in the construction of the self-assembled structures comprising a

Fig. 5 GISAXS patterns corresponding to (a) (OsPA/GOx)$_3$ and (b) (OsPA/SDS/OsPA/GOx)$_3$ multilayers. GISAXS experiments were performed at room temperature and RH: 20%. The color scale of both diagrams are identical and the angle of incidence (relative to the film surface) α_i was 0.17°.
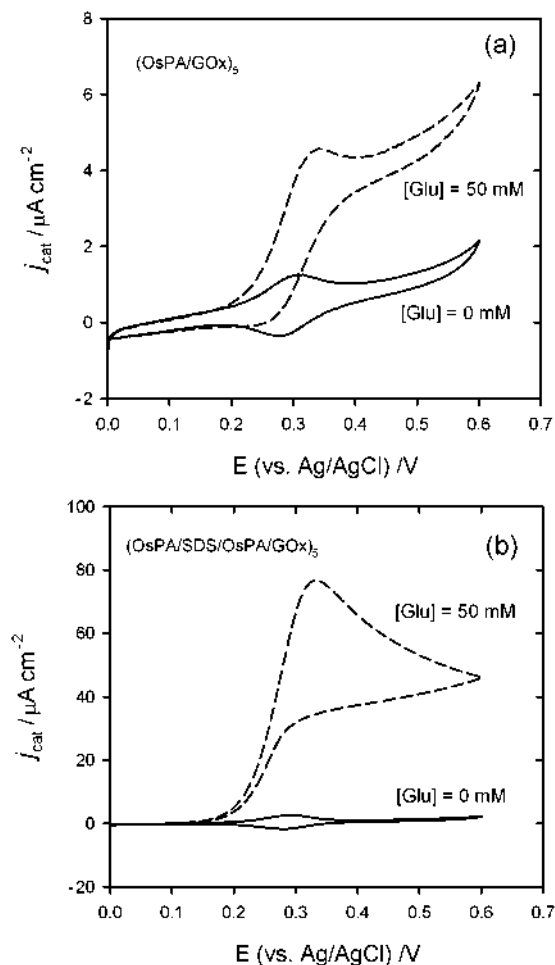
This journal is © the Owner Societies 2014

Phys. Chem. Chem. Phys., 2014, 16, 20844–20855 | 20849

Fig. 8 Bioelectrocatalytic current as a function of GOx layers incorporated into the supramolecular assembly for $(OsPA/GOx)_n$ (○) and (OsPA/SDS/OsPA/GOx)$_n$ (●). Bioelectrochemical experiments were performed in the presence of 50 mM glucose in 50 mM HEPES, 0.2 M KNO_3 buffer solution at pH 7.0. Error bars are smaller than the symbol size.

Fig. 7 Voltammetric response of (a) $(OsPA/GOx)_5$ and (b) (OsPA/SDS/OsPA/GOx)$_5$ multilayers in the absence and in the presence of 50 mM glucose in 50 mM HEPES, 0.2 M KNO_3 buffer solution at pH 7.0. The voltammograms are depicted in different traces for the sake of clarity. Temperature: 298 K and scan rate: 10 mV s^{-1}.

redox-active electrolyte and GOx allows the incorporation of a greater amount of each species. In the case of OsPA we observed that even though the content of the redox polyelectrolyte in the assemblies is higher in (OsPA/SDS/OsPA/GOx)$_n$ the population of redox active centers is the same in both type of assemblies. On the other hand, we have estimated that the content of GOx is 2.8 times higher in (OsPA/SDS/OsPA/GOx)$_n$ films with respect to $(OsPA/GOx)_n$. In principle the sensitivities of these enzyme electrodes is controlled by the amounts of protein immobilized onto the electrodes. An estimation of glucose responsiveness from data displayed in Fig. 8 reveals sensitivities of 18.4 and 2.1 μA cm^{-2} per added GOx layer for (OsPA/SDS/OsPA/GOx)$_n$ and $(OsPA/GOx)_n$ assemblies, respectively. This suggests that for the same population of redox active centers, a 3-fold increase in enzyme coverage in SDS-containing assemblies led to sensitivity enhancement by a factor of 9. We attribute the marked improvement in the catalytic current to a better interaction between the enzyme and the polyelectrolyte due to the presence of SDS.

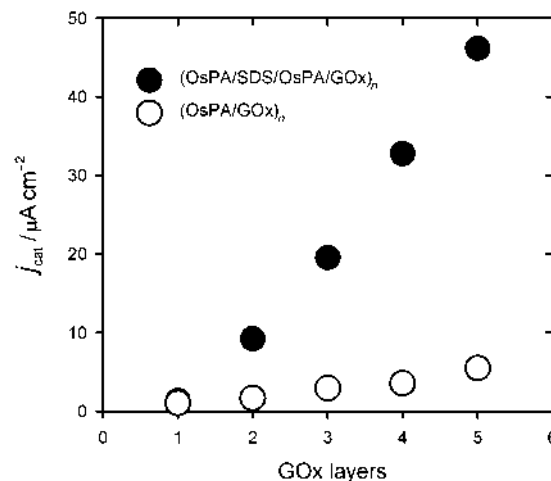By following the same line of reasoning that led us to the integration of SDS in the LBL assembly we proceeded to assemble analogue systems integrating sodium octadecylsulfate (ODS) instead of shorter-chain SDS. ODS represents a long-chain amphiphilic molecule that could confer a more hydrophobic character to the film with the concomitant effect on the adsorption of GOx. Fig. 9a shows the cyclic voltammogram corresponding to the bioelectrocatalytic current of a (OsPA/ODS/OsPA/GOx)$_1$-modified electrode in the presence of 50 mM glucose. Clearly, an electrocatalytic anodic current is observed at the oxidation potential of Os centers. This bioelectrocatalytic current is significantly larger than that measured on (OsPA/SDS/OsPA/GOx)$_1$-modified electrodes. This fact would indicate that the increased hydrophobicity of ODS-containing films play a role in the enhancement of the bioelectrochemical signal. Indeed, QCM data confirmed that the amount of GOx immobilized during the first adsorption step is significantly larger than that observed in SDS-containing films, i.e. 1.47 versus 0.53 μg cm^{-2}. Thereafter, continuing the multilayer buildup through a second dipping cycle a very interesting fact was revealed. Surprisingly, the bioelectrocatalytic current measured in (OsPA/ODS/OsPA/GOx)$_2$ assemblies is much lower than that measured in (OsPA/ODS/OsPA/GOx)$_1$-modified electrodes. In addition, cyclic voltammograms in the absence of glucose indicate that the population of "wired" redox centers does not increase after adding a second composite layer although QCM data indicated that during the second dipping cycle 1.07 μg cm^{-2} of OsPA and 2.47 μg cm^{-2} of GOx were integrated in the multilayer assembly. These electrochemical results strongly suggest that in the case of ODS-containing films the multilayer buildup has a detrimental effect on the functional properties of the biofunctional assembly.

A direct comparison of electrocatalytic currents measured in $(OsPA/GOx)_n$, (OsPA/SDS/OsPA/GOx)$_n$ and (OsPA/ODS/OsPA/GOx)$_n$ multilayers during the first two dipping cycles unequivocally reveals the strong influence of the surfactant on the bioelectrocatalytic functional properties (see Fig. 10).
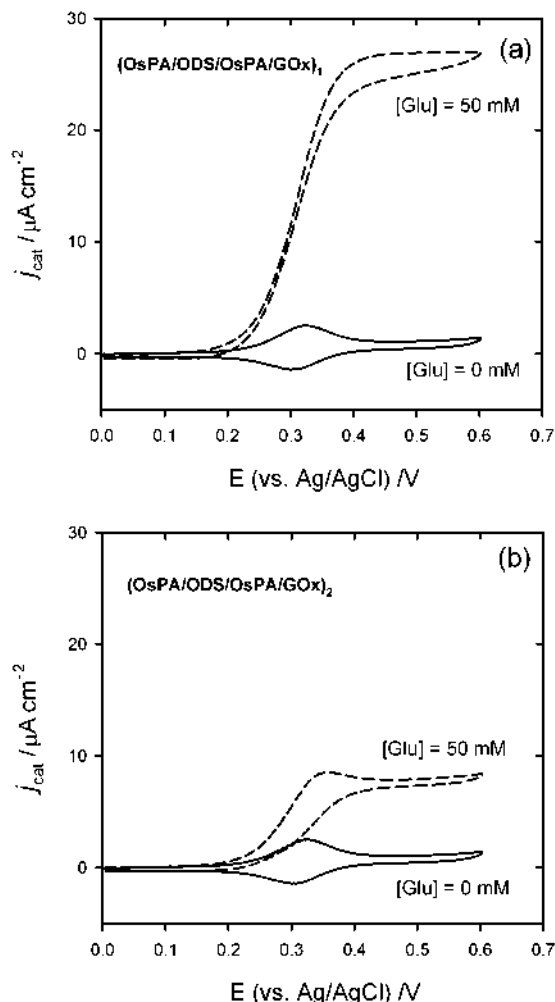
20850 | Phys. Chem. Chem. Phys., 2014, **16**, 20844–20855

This journal is © the Owner Societies 2014

Fig. 9 Voltammetric response of (a) (OsPA/ODS/OsPA/GOx)$_1$ and (b) (OsPA/ODS/OsPA/GOx)$_2$ multilayers in the absence and in the presence of 50 mM glucose in 50 mM HEPES, 0.2 M KNO$_3$ buffer solution at pH 7.0. The voltammograms are depicted in different traces for the sake of clarity. Temperature: 298 K and scan rate: 10 mV s^{-1}.
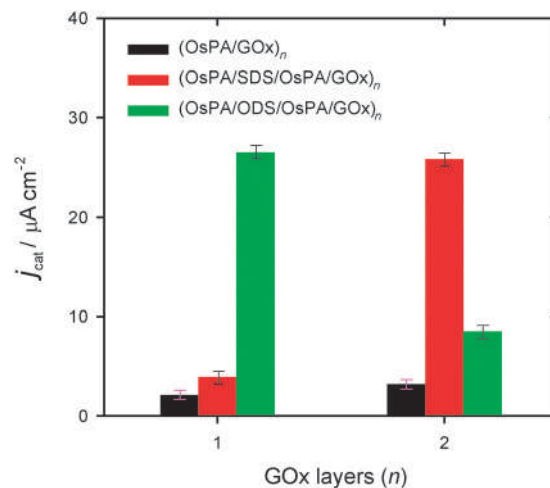

Fig. 10 Comparative chart describing variations in bioelectrocatalytic currents for multilayers containing one and two GOx layers integrated in surfactant-free, SDS- and ODS-containing multilayers.
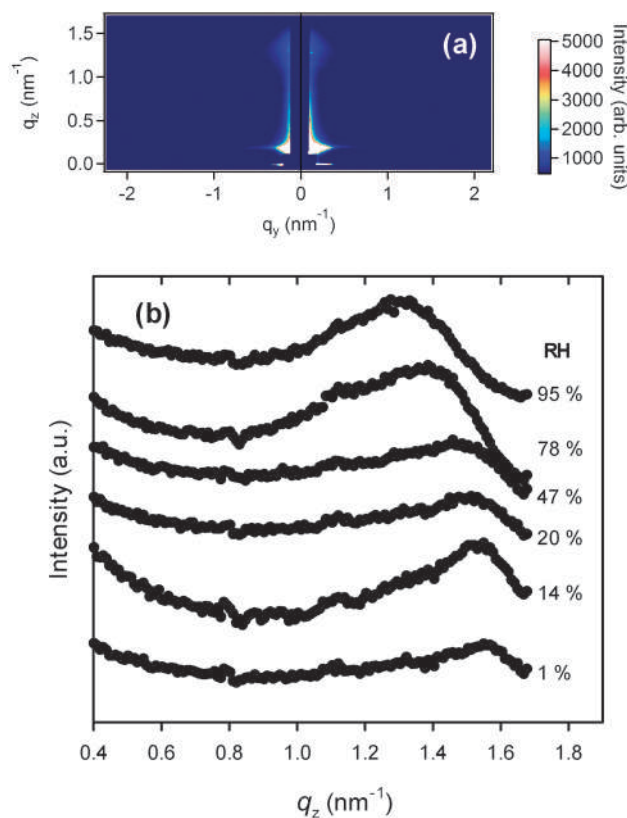

Fig. 11 (a) GISAXS pattern corresponding to a (OsPA/ODS/OsPA/GOx)$_2$ multilayer assembly obtained under ambient conditions (RH: 20%, the angle of incidence of the beam α_i was 0.17°). (b) Out-of-plane scattering profiles extracted along the q_z direction (at q_y = 0.2 nm^{-1}) from the GISAXS patterns of (OsPA/SDS/OsPA/GOx)$_2$ multilayers obtained under different humidity conditions.

The present question is whether the presence of ODS in the LbL assembly would significantly affect the mesoorganization in such a way that promotes a dramatic effect on the electrochemical activity of redox-active film. In order to answer this question, we further studied the mesoorganization of (OsPA/ODS/OsPA/GOx)$_2$ films under different humidity conditions (Fig. 11).

GISAXS characterization conclusively confirmed the presence of lamellar domains strongly oriented parallel to the substrate. In fact, the absence of a halo further suggests that ODS acts as an efficient mesostructure-directing agent inhibiting the formation of multi-oriented domains. It is evident that the surfactant alkyl chain length plays a role in defining not only the film mesostructure but also the water uptake characteristics in aqueous environments. These are crucial aspects to understand the electrochemical behavior of the redox centers confined in the polyelectrolyte domains. Fig. 12 depicts changes in lamellar spacing in (OsPA/ODS/OsPA/GOx)$_2$ films under different humidity conditions. For the sake of

comparison, data from (OsPA/SDS/OsPA/GOx)$_2$ were also included in the plot. We observe that in the presence of water (OsPA/ODS/OsPA/GOx)$_2$ assemblies display significant swelling of the

This journal is © the Owner Societies 2014

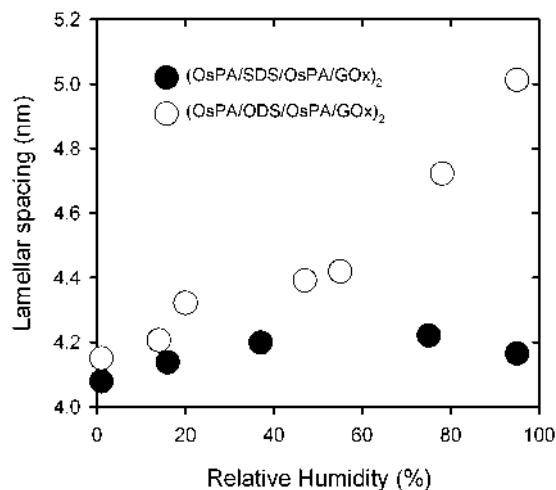Phys. Chem. Chem. Phys., 2014, 16, 20844–20855 | 20851

Fig. 12 Representation of the lamellar spacing of the mesostructured assemblies as a function of relative humidity: (○) (OsPA/ODS/OsPA/GOx)$_2$ and (●) (OsPA/SDS/OsPA/GOx)$_2$. The error bars are smaller than the symbol size.
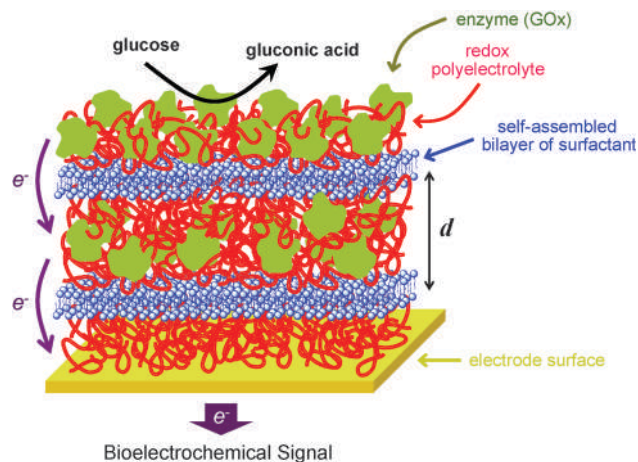

Fig. 13 Simplified schematic of the glucose-responsive ternary supramolecular architecture. Poly(allylamine) containing an osmium polypyridil complex (OsPA), octadecyl sulfate (ODS) and glucose oxidase (GOx) are spontaneously assembled via electrostatic and hydrophobic interactions onto electrode surfaces. The figure displays the constituting building blocks (not to scale) participating in the generation of the bioelectrochemical signal in the presence of glucose as well as a simplified view of their organization in the interfacial architecture. The distance d refers to the lamellar spacing estimated from GISAXS experiments.

polyelectrolyte domains. Indeed, lamellar spacing increases from 4.15 to 5.00 nm upon increasing the humidity from 1 to 95% ($\sim$18% increase). Contrarily, SDS-containing films exhibit a much less pronounced change in lamellar spacing when subjected to similar conditions.

These figures translate into important implications for charge transport within the film. To understand how the meso-organization of redox centers confined into the film affects the electron transport we need to consider GISAXS patterns in water-saturated environments. In the case of (OsPA/ODS/OsPA/GOx)$_n$ films a strong anisotropy in the intensity distribution arises due to in-plane confinement effects. Because of this effect, swelling of the lamellae in the in-plane direction is limited, whereas that in the direction normal to the substrate (out-of-plane) is unconfined; this results in greater levels of swelling from domains with periodicity in the out-of-plane direction as evidenced by higher

scattering intensity in the GISAXS patterns away from the specular position. This scenario implies that octadecyl sulfate molecules strongly favor the stratification of the redox-active polyelectrolyte domains and at the same time the surfactant bilayers formed by octadecyl chains act as spacers between electroactive regions (Fig. 13). The convolution of both effects has a detrimental effect on the electron transfer across the film if we consider that electron hopping, and even tunneling, is strongly inhibited in the presence of long insulating aliphatic chains, i.e.: octadecyl chains.

On the other hand, (OsPA/SDS/OsPA/GOx)$_n$ assemblies exhibit a much less anisotropic scattering thus suggesting that swelling of multi-oriented lamellar domains can take place in both
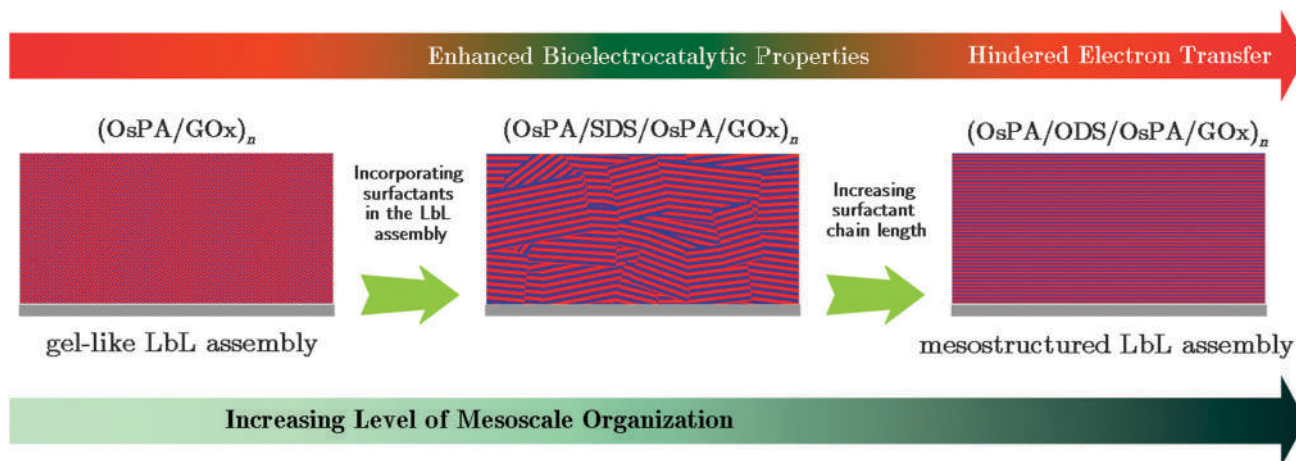

Fig. 14 Schematic describing the mesoorganization of surfactant-free and surfactant-containing layer-by-layer assemblies. Simplified cartoons are depicted according to experimental results obtained from GISAXS characterization.

in-plane and out-of-plane directions. This might lead to a situation in which electron hopping between Os centers can take place in hydrophilic domains percolating across the boundaries of multi-oriented lamellae. This picture closely resembles the formation of highly ion- and water-conductive channels in Nafion films. In our case the LbL assembly leads to the mesostructural organization of structural domains and redox conducting domains into which enzymes are hosted.

In general terms, according to our structural characterization, integration of SDS in the LbL assembly confers short-range mesoorganization to the typical gel-like (OsPA/GOx) assembly (Fig. 14). The presence of the amphiphilic molecules leads to phase separation between redox conducting and structural domains as well as an increase in protein and polyelectrolyte coverage due to the dominant role of hydrophobic forces. As the alkyl chains of the surfactants increase in length, supramolecular assemblies show a higher degree of mesoorganization with the concomitant increase in the order of redox conducting domains oriented parallel to the electrode surface. This new scenario is completely different from the classical notion of redox-active hydrogel-like LbL assemblies in which the electron transfer efficiency, *i.e.* redox "wiring", is almost exclusively dominated by the swelling/shrinking of the hydrogel.[68]

Conclusions

The preparation of mesostructured layered assemblies integrating redox proteins and displaying optimized functional properties is important for both fundamental materials research and practical applications of bioelectrochemistry. These results using supramolecular assemblies based on redox-active polyelectrolytes, enzymes and surfactants demonstrate the potential of using LbL as a key enabling tool granting access to the rational molecular design of complex interfacial assemblies. In summary, we want to emphasize three points, which appear to be the most significant aspects of our investigation: (1) surfactants in LbL films play a dual role as mesomorphic structure-directing agents as well as a driving force to increase the adsorption of the enzyme through hydrophobic interactions; (2) there is a trade-off between enzyme coverage and the bioelectrocatalytic signal that is governed by the meso-organization and hydrophobic characteristics of the multilayer assembly; and (3) hydrophobic interactions may dictate 3D organization of multilayer assemblies and lead to major changes in functional properties.

The present study demonstrated the superior bioelectrocatalytic properties through the $(OsPA/SDS/OsPA/GOx)_n$ composite system as compared to the traditional $(OsPA/GOx)_n$ system. The enhanced bioelectrocatalytic functions of the $(OsPA/SDS/OsPA/GOx)_n$ composite material originate from the increased masses of the protein and redox polyelectrolyte adsorbed on the hydrophobic multilayer assemblies. Charge hopping within the composite (OsPA/SDS/OsPA/GOx) assembly proceeds through the boundaries of multi-oriented lamellar redox domains.

Upon further increasing the length of the surfactant alkyl chain, the degree of lamellar organization increases as observed in GISAXS experiments. Similarly, protein coverage increases upon increasing the surfactant alkyl chain. Hydrophobic interactions between the hydrocarbon tails of the surfactants and polyelectrolyte and/or proteins significantly increase the attractive component of the surfactant–polyelectrolyte and surfactant–enzyme interactions. However, the formation of well-organized lamellar domains oriented parallel to the electrode surface leads to composite assemblies with poor bioelectrocatalytic properties. This observation has been ascribed to the presence of long alkyl chains located between organized redox domains that act as spacers precluding the electron transfer among electroactive sites. These findings are important for understanding the interdependence of forces resulting in the layer-by-layer buildup, rational selection of the surfactant–polyelectrolyte systems, and control of the structure of the multilayer. From a preparative point of view, the elegance of this assembly approach lies in the rational choice of individual components that, in turn, determine the overall features of the whole bioelectroactive assembly. This concept represents a crucial feature for the nanoconstruction of bioelectronic interfaces as well as the development of amperometric biosensors with higher sensitivity and biofuel cells with larger current values.

Acknowledgements

References

1 I. Willner, R. Tel-Vered and B. Willner, *Engineering the Bioelectronic Interface*, ed. J. Davis, Royal Society of Chemistry, Cambridge, 2009, ch. 3, pp. 56–118.

2 *Biomolecular Films: Design, Function and Applications*, ed. J. F. Rusling, Marcel Dekker, New York, 2003.

3 R. Tel-Vered, B. Willner and I. Willner, in *Electrochemistry of Functional Supramolecular Systems*, ed. P. Ceroni, A. Credi and M. Venturi, John Wiley & Sons, Hoboken, 2010, ch. 12, pp. 333–376.

4 (*a*) D. T. Balogh, M. Ferreira and O. N. Oliveria, in *Functional Polymer Films*, ed. R. C. Advincula and W. Knoll, VCH-Wiley, Weinheim, 2011, ch. 4, vol. 1, pp. 113–149; (*b*) J. H. Park and R. C. Advincula, *Soft Matter*, 2011, 7, 9829–9843.

This journal is © the Owner Societies 2014

Phys. Chem. Chem. Phys., 2014, **16**, 20844–20855 | 20853

5 K. Sakakibara, J. P. Hill and K. Ariga, *Small*, 2011, **7**, 1288–1308.

6 K. Ariga, Q. Ji, T. Mori, M. Naito, Y. Yamauchi, H. Abe and J. P. Hill, *Chem. Soc. Rev.*, 2013, **42**, 6322–6345.

7 M. Aono, Y. Bando and K. Ariga, *Adv. Mater.*, 2012, **24**, 150–151.

8 K. Ariga, M. V. Lee, T. Mori, X.-Y. Yu and J. P. Hill, *Adv. Colloid Interface Sci.*, 2010, **154**, 20–29.

9 M. Ramanathan, L. K. Shrestha, T. Mori, Q. Ji, J. P. Hill and K. Ariga, *Phys. Chem. Chem. Phys.*, 2013, **15**, 10580–10611.

10 *Manipulation of Nanoscale Materials: An Introduction to Nanoarchitectonics*, ed. K. Ariga, Royal Society of Chemistry, Cambridge, 2012.

11 *Langmuir Monolayers in Thin Films Technology*, ed. J. A. Sherwin, Nova Science Publishers, New York, 2011.

12 I. Willner and B. Willner, *J. Mater. Chem.*, 1998, **8**, 2543–2556.

13 A. Ulman, *Introduction to Ultrathin Organic Films: From Langmuir-Blodgett to Self-Assembly*, Academic Press, San Diego, 1991.

14 A. N. Shipway, M. Lahav and I. Willner, *Adv. Mater.*, 2000, **12**, 993–998.

15 K. Ariga, J. P. Hill and Q. Ji, *Phys. Chem. Chem. Phys.*, 2007, **9**, 2319–2340.

16 O. Crespo-Biel, B. Dordi, D. N. Reinhoudt and J. Huskens, *J. Am. Chem. Soc.*, 2005, **127**, 7594–7600.

17 (*a*) G. Decher and J. D. Hong, *Ber. Bunsen-Ges.*, 1991, **95**, 1430–1434; (*b*) G. Decher and J. D. Hong, *Makromol. Chem., Macromol. Symp.*, 1991, **46**, 321–327.

18 (*a*) G. Decher, *Multilayer Thin Films*, ed. G. Decher and J. B. Schlenoff, Wiley-VCH, Weinheim, 2002, ch. 1, pp. 1–46; (*b*) X. Shia, M. Shen and H. Möhwald, *Prog. Polym. Sci.*, 2004, **29**, 987–1019.

19 (*a*) K. Ariga, Q. Ji, J. P. Hill and A. Vinu, *Soft Matter*, 2009, **5**, 3562–3571; (*b*) P. Bertrand, A. M. Jonas, A. Laschewsky and R. Legras, *Macromol. Rapid Commun.*, 2000, **21**, 319–348.

20 M. Coustet, J. Irigoyen, T. Alonso Garcia, R. A. Murray, G. Romero, M. S. Cortizo, W. Knoll, O. Azzaroni and S. E. Moya, *J. Colloid Interface Sci.*, 2014, **421**, 132–140.

21 O. Azzaroni and K. H. A. Lau, *Soft Matter*, 2011, **7**, 8709–8724.

22 M. Ali, B. Yameen, J. Cervera, P. Ramírez, R. Neumann, W. Ensinger, W. Knoll and O. Azzaroni, *J. Am. Chem. Soc.*, 2010, **132**, 8338–8348.

23 E. Katz and I. Willner, *Angew. Chem., Int. Ed.*, 2004, **43**, 6042–6108.

24 M. L. Cortez, G. A. González, M. Ceolín, O. Azzaroni and F. Battaglini, *Electrochim. Acta*, 2014, **118**, 124–129.

25 M. L. Cortez, D. Pallarola, M. Ceolín, O. Azzaroni and F. Battaglini, *Anal. Chem.*, 2013, **85**, 2414–2422.

26 M. L. Cortez, D. Pallarola, M. Ceolín, O. Azzaroni and F. Battaglini, *Chem. Commun.*, 2012, **48**, 10868–10870.

27 D. Pallarola, N. Queralto, W. Knoll, M. Ceolín, O. Azzaroni and F. Battaglini, *Langmuir*, 2010, **26**, 13684–13696.

28 (*a*) E. J. Calvo, C. Danilowicz and A. Wolosiuk, *J. Am. Chem. Soc.*, 2002, **124**, 2452–2453; (*b*) V. Flexer, E. S. Forzani, E. J. Calvo, S. J. Ludueña and L. I. Pietrasanta, *Anal. Chem.*, 2006, **78**, 399–407.

29 N. Kotov, *Nanostruct. Mater.*, 1999, **12**, 789–796.

30 *Self-Assembled Supramolecular Architectures*, ed. N. Garti, P. Somasundaranand and R. Mezzenga, John Wiley & Sons, Hoboken, 2012.

31 (*a*) T. Abraham and S. Giasson, *Colloids Surf., A*, 2001, **180**, 103–110; (*b*) A. Dedinaite, P. M. Claesson and M. Bergström, *Langmuir*, 2000, **16**, 5257–5266; (*c*) P. M. Claesson, A. Dedinaite, E. Blomberg and V. G. Sergeyev, *Ber. Bunsen-Ges. Phys. Chem.*, 1996, **100**, 1008–1013.

32 M. A. Rahim, W. S. Choi, H.-J. Lee and I. C. Jeon, *Langmuir*, 2010, **26**, 4680–4686.

33 *Functional Hybrid Materials*, ed. P. Gómez-Romero and C. Sanchez, Wiley-VCH, Weinheim, 2004.

34 *Liquid Crystalline Functional Assemblies and Their Supramolecular Structures*, ed. T. Kato, Springer Verlag, Heidelberg, 2008.

35 *Structured Fluids: Polymers, Colloids, Surfactants*, ed. T. Witten and P. Pincus, Oxford University Press, Oxford, 2004.

36 W. J. Macknight, E. A. Ponomarenko and D. A. Tirrell, *Acc. Chem. Res.*, 1998, **31**, 781–788.

37 M. S. Johal and P. A. Chiarelli, *Soft Matter*, 2007, **3**, 34–46.

38 X. Arys, P. Fischer, A. M. Jonas, M. M. Koetse, A. Laschewsky, R. Legras and E. Wischerhoff, *J. Am. Chem. Soc.*, 2003, **125**, 1859–1865.

39 A. Arys, L. Laschewsky and A. M. Jonas, *Macromolecules*, 2001, **34**, 3318–3330.

40 (*a*) S. Joly, R. Kane, L. Radzilowski, T. Wang, A. Wu, R. E. Cohen, E. L. Thomas and M. F. Rubner, *Langmuir*, 2000, **16**, 1354–1359; (*b*) A. Wu, D. Yoo, J. K. Lee and M. F. Rubner, *J. Am. Chem. Soc.*, 1999, **121**, 4883–4891; (*c*) J. B. Schlenoff, H. Ly and M. Li, *J. Am. Chem. Soc.*, 1998, **120**, 7626–7634; (*d*) G. J. Kellogg, A. M. Mayes, W. B. Stockton, M. Ferreira, M. F. Rubner and S. K. Satija, *Langmuir*, 1996, **12**, 5109–5113; (*e*) M. Lösche, J. Schmitt, G. Decher, W. G. Bouwman and K. Kjaer, *Macromolecules*, 1998, **31**, 8893–8906.

41 D. Pallarola, C. von Bildering, L. I. Pietrasanta, N. Queralto, W. Knoll, F. Battaglini and O. Azzaroni, *Phys. Chem. Chem. Phys.*, 2012, **14**, 11027–11039.

42 D. Pallarola, N. Queralto, W. Knoll, O. Azzaroni and F. Battaglini, *Chem. – Eur. J.*, 2010, **16**, 13970–13975.

43 (*a*) X. Liu, L. Zhou, W. Geng and J. Sun, *Langmuir*, 2008, **24**, 12986–12989; (*b*) I. P. Sergeeva, V. D. Sobolev, G. A. Dibrov and N. V. Churaev, *Colloid J.*, 2011, **73**, 378–383.

44 M. Lorena Cortez, A. L. Cukierman and F. Battaglini, *Electrochem. Commun.*, 2009, **11**, 990–993.

45 C. Danilowicz, E. Cortón and F. Battaglini, *J. Electroanal. Chem.*, 1998, **445**, 89–94.

46 G. Z. Sauerbrey, *Z. Phys.*, 1959, **155**, 206–222.

47 V. Flexer, M. V. Ielmini, E. J. Calvo and P. N. Bartlett, *Bioelectrochemistry*, 2008, **74**, 201–209.

48 Z. Di, D. Posselt, D.-M. Smilgies, R. Li, M. Rauscher, I. I. Potemkin and C. M. Papadakis, *Macromolecules*, 2012, **45**, 5185–5195.

49 O. Azzaroni, M. Álvarez, A. I. Abou-Kandil, B. Yameen and W. Knoll, *Adv. Funct. Mater.*, 2008, **18**, 3487–3496.

50 M. A. Rahim, W. S. Choi, H.-J. Lee and I. C. Jeon, *Langmuir*, 2010, **26**, 4680–4686.

51 O. Azzaroni, M. Mir and W. Knoll, *J. Phys. Chem. B*, 2007, **111**, 13499–13503.

52 N. Cheng, O. Azzaroni, S. E. Moya and W. T. S. Huck, *Macromol. Rapid Commun.*, 2006, **27**, 1632–1636.

53 S. Moya, A. A. Brown, O. Azzaroni and W. T. S. Huck, *Macromol. Rapid Commun.*, 2005, **26**, 1117–1121.

54 *Interfacial Supramolecular Assemblies*, ed. J. G. Vos, R. J. Forster and T. E. Keyes, John Wiley & Sons, Hoboken, 2003.

55 C. D. Bain, P. M. Claesson, D. Langevin, R. Meszaros, T. Nylander, C. Stubenrauch, S. Titmuss and R. von Klitzing, *Adv. Colloid Interface Sci.*, 2010, **155**, 32–49.

56 M. S. Johal, B. H. Ozer, J. L. Casson, A. St. John, J. M. Robinson and H.-L. Wang, *Langmuir*, 2004, **20**, 2792–2796.

57 M. N. Jones, P. Manley and A. Wilkinson, *Biochem. J.*, 1982, **203**, 285–291.

58 E. J. Calvo, R. Etchenique, L. Pietrasanta, A. Wolosiuk and C. Danilowicz, *Anal. Chem.*, 2001, **73**, 1161–1168.

59 P. Müller-Buschbaum, *Adv. Mater.*, 2014, DOI: 10.1002/adma.201304187.

60 G. Renaud, R. Lazzari and F. Leroy, *Surf. Sci. Rep.*, 2009, **64**, 255–380.

61 P. Busch, D. Posselt, D.-M. Smilgies, M. Rauscher and C. M. Papadakis, *Macromolecules*, 2007, **40**, 630–640.

62 M. A. Modestino, D. K. Paul, S. Dishari, S. A. Petrina, F. I. Allen, M. A. Hickner, K. Karan, R. A. Segalman and A. Z. Weber, *Macromolecules*, 2013, **46**, 867–873.

63 M. A. Modestino, A. Kusoglu, A. Hexemer, A. Z. Weber and R. A. Segalman, *Macromolecules*, 2012, **45**, 4681–4688.

64 J. Bolze, M. Takahasi, J. Mizuki, T. Baumgart and W. Knoll, *J. Am. Chem. Soc.*, 2002, **124**, 9412–9421.

65 M. L. Cortez, M. Ceolín, O. Azzaroni and F. Battaglini, *Anal. Chem.*, 2011, **83**, 8011–8018.

66 *Supramolecular Design for Biological Applications*, ed. N. Yui, CRC Press, Boca Raton, 2002.

67 *Biopolymers at Interfaces*, ed. M. Malmsten, Marcel Dekker, New York, 2003.

68 (*a*) F. Battaglini, E. J. Calvo, C. Danilowicz and A. Wolosiuk, *Anal. Chem.*, 1999, **71**, 1062–1067; (*b*) A. Heller, *Acc. Chem. Res.*, 1990, **23**, 128–134.